

THE ORIGIN OF EXTREME HORIZONTAL BRANCH STARS

Noella L. D’Cruz¹

Ben Dorman^{1,2}

Robert T. Rood¹

Robert W. O’Connell¹

University of Virginia, P.O. Box 3818, Charlottesville, VA 22903

Submitted to the Astrophysical Journal

ABSTRACT

Strong mass loss on the red giant branch (RGB) can result in the formation of extreme horizontal branch (EHB) stars. The EHB stars spend most of their He core & shell burning phase at high temperatures and produce copious ultraviolet flux. They have very small hydrogen envelopes and occupy a small range in mass. It has been suggested that the ultraviolet excess phenomenon, seen in elliptical galaxies and spiral bulges, is largely due to the ultraviolet flux from EHB stars and their progeny. The main motivation behind this work is to understand how EHB stars can be produced over a wide range of metallicities without fine tuning the mass loss process.

We have computed evolutionary RGB models with mass loss for stars with main sequence ages between 12.5 and 14.5 Gyr, initial masses $< 1.1M_{\odot}$ and metallicities of $[\text{Fe}/\text{H}] = -2.26, -1.48, -0.78, 0.0, \text{ and } 0.37$. We used the Reimers formula to characterize mass loss, but investigated a larger range of the mass loss efficiency parameter, η_R , than is common. We adopted values of η_R from 0 to 1.2 for the compositions considered. Sufficiently rapid RGB mass loss causes stars to “peel-off” the giant branch, evolve to high temperatures and settle on the white dwarf cooling curve. Some such stars have adequate helium core mass to undergo the helium flash, but only later at high temperatures: we call these “hot He-flashers”. After helium ignition, the hot flashers lie at the very blue end of the horizontal branch, forming a “blue hook.” The blue hook stars are a part of the EHB population and evolve into AGB-manqué stars. The rest of the peel-off stars form helium white dwarfs which we call “flash-manqué” stars. To understand how the number of EHB stars varies with metallicity in a stellar population we considered how the zero-age horizontal branch (ZAHB) is populated. We assumed the distribution of ZAHB stars to be driven by a distribution in the mass loss efficiency (parametrized by η_R) rather than

¹nld2n@virginia.edu; dorman@shemesh.gsfc.nasa.gov; rtr@virginia.edu; rwo@virginia.edu

²Present Address: Laboratory for Astronomy and Solar Physics, Code 681, NASA Goddard Space Flight Center, Greenbelt, MA 20771

by a distribution in mass. Our results show that at low metallicity, EHB stars are produced if η_R is 2–3 times larger than the value producing normal “mid-HB stars.” However the range in η_R producing EHB stars is comparable to that producing mid-HB stars. Somewhat surprisingly, neither the range nor magnitude of η_R producing EHB stars varies much metallicity. In contrast, the range of η_R producing mid-HB stars decreases with increasing metallicity. Hence the HB of populations with solar metallicity and higher, such as expected in elliptical galaxies and spiral bulges, will be bimodal if the distribution covers a sufficiently large range in η_R .

Subject headings: galaxy: globular clusters: general—galaxy: open clusters and associations—stars: horizontal branch—stars: giants— stars: evolution—stars: mass loss—stars: Population II—ultraviolet: galaxies—ultraviolet: stars

1. INTRODUCTION

Extreme horizontal branch (EHB) are stars which fail to reach the thermally pulsing stage on the asymptotic giant branch (AGB) after evolving off the zero-age horizontal branch (ZAHB). After core helium exhaustion, EHB stars evolve into either Post-Early AGB (P-EAGB) stars which leave the AGB before thermal pulsing or AGB-manqué stars, which never reach the AGB (Brocato, et al. 1990; Greggio & Renzini 1990 [GR90]; Dorman, Rood, & O’Connell 1993 [DOR93]). These stars have undergone such extreme mass loss during their first ascent up the giant branch that only a very thin hydrogen envelope survives. Stars identified as EHB stars are found in low metallicity globular clusters as an extension of the normal HB—perhaps most prominently in ω Cen (Whitney et al. 1994) and NGC 6752 (Buonanno et al. 1986; Castellani, Degli’Innocenti, & Pulone 1995). In higher metallicity populations, EHB stars are found in the metal rich cluster NGC 6791 (Liebert, Saffer, & Green 1994) and as field sdB stars (Saffer & Liebert 1995; Dorman, O’Connell, & Rood 1995 [DOR95]). EHB stars and their AGB-manqué and P-EAGB progeny are perhaps the prime candidate objects for the far-ultraviolet upturn (UVX) observed in elliptical galaxies and spiral galaxy bulges (Burstein et al. 1988; GR90; Ferguson & Davidsen 1993; DOR95).

One difficulty in understanding the EHB stars is that at a given composition the range of total stellar mass which produces EHB behavior is very narrow. Superficially, it appears that mass loss must be “fine tuned” such that the red giants lose a large amount of mass, but stop just short of losing the entire envelope. For globular clusters where the blue HB is populated (the intermediate blue HB (IBHB) in the nomenclature of DOR95) it is easy to imagine that some EHB stars result from the high mass loss tail of the mass loss distribution. At high metallicity as in NGC 6791 ($[\text{Fe}/\text{H}] \sim +0.2$) there appear to be EHB stars even though the IBHB is not populated—Liebert et al. (1994) were unable to explain NGC 6791 with a “normal” HB mass distribution. Also, the sdB stars of the Galactic field form a separate evolutionary group from the field blue HB stars (Heber 1986) and make up a considerable proportion of all UV-excess objects (Green, Schmidt, & Liebert 1986). Since the EHB appears to occur over a wide range of metallicity, not only might the mass loss require “tuning,” but that tuning might require substantial adjustment with metallicity. Understanding how EHB stars could be produced for a wide range of compositions, without fine tuning, was the initial motivation for this investigation.

The effects of mass loss have been studied extensively in the different phases of stellar evolution (see Dupree 1986 for a review). If the sun is to be taken as an example, low mass main sequence (MS) stars experience negligible mass loss, $\sim 10^{-14} M_{\odot} \text{ yr}^{-1}$. If the rate of mass loss is constant over the main sequence lifetime of a star then it loses on the order of $10^{-4} M_{\odot}$ in about 10 Gyr. However, the mass loss rate is expected to increase as stellar luminosity increases and surface gravity decreases along the giant branch. Both observations and empirical scaling laws such as the Reimers’ relation (Reimers 1975, 1977) suggest that a substantial fraction of a star’s mass could be lost on the giant branch (Dupree 1986). Since mass loss is a surface phenomenon, it only affects the convective envelope of the RGB stars, and except in extreme cases, evolution of the interior of the star continues without any knowledge of the loss of the mass from the surface (see also Jimenez et al. 1995 and Castellani & Castellani 1993 [CC93]). Because of this, mass loss has ordinarily been neglected during red giant evolution, with the total mass lost during this phase being removed at the helium flash for the purposes of modeling later evolution.

However, with extreme, but plausible mass loss rates, a star can lose so much mass that its total mass becomes comparable to its core mass. The basic behavior of such stars is obvious (Renzini 1981; Caputo et al. 1981). At some point the envelope mass becomes so small that a large convective envelope can no longer exist. Then, instead of continuing to the tip of the giant branch, the star “peels-off” the giant branch and evolves towards higher temperatures at almost constant luminosity. We call this an RGB peel-off star.

There are two possible routes of evolution for peel-off stars. The more obvious resembles the evolution of Post-AGB models (Schönberner 1979, 1983) but with the peel-off stars dying quietly as He white dwarfs (He WDs). We refer to these as “flash-manqué” stars (RGB-stragglers in the nomenclature of Luridiana 1994 and Castellani, Luridiana, & Romaniello 1994). Initially, it was assumed that this was the only route followed by peel-off stars. Hence, it was also assumed that the smallest envelope mass that actually reaches the He-flash on the RGB, i.e. the envelope mass at peel-off, set the minimum envelope mass — and thus the maximum effective temperature — for HB stars at the onset of He burning. Eventually CC93 found another evolutionary path for peel-off stars. Despite the fact that the stars were cooling along the He-white-dwarf cooling curve, for some range of parameters a He core flash occurred. Even though the H-burning shell was extinguished, the outer parts of He core were compressible enough that contraction continued, leading eventually to helium ignition. We call these stars “hot He-flashers” to distinguish them from the classic RGB tip flashers. Hot-flashers spend their entire He burning life at high T_{eff} , first as extreme HB stars, and then as AGB-manqué stars (CC93; Castellani et al. 1995).

CC93 discovered hot-flashers in a study which incorporated mass loss along the giant branch via the Reimers formula (Reimers 1977). From CC93 as well as Castellani et al. (1994) and Castellani et al. (1995), it was not clear whether hot-flash behavior could be achieved without fine tuning the Reimers mass loss efficiency η_R . Our initial goal was to determine the range of η_R leading to the high-temperature flashes as a function of metallicity. Anticipating that fine tuning would be required, we would then explore other mass loss formalisms which would more easily lead to the production of EHB stars. As it turned out, fine tuning of η_R was not necessary. We expect that the hot-flash phenomenon should occur for a fairly broad class of mass loss laws for almost any composition.

We have computed RGB models with mass loss over a wide range of metallicities. The calculations of our models, including our treatment of mass loss are described in § 2. We present the results of our RGB models and their corresponding HB models in § 2.2 and § 2.3 respectively. The astrophysical significance of our results and the occurrence of EHB stars in stellar populations with different metallicities is discussed in § 3. The conclusions are summarized in § 4.

2. CALCULATIONS

2.1. Procedures

We have computed evolutionary tracks from the zero-age main sequence (ZAMS), using a modified version of the stellar evolution code STEV (Dorman 1992a). The details of the code can be found in

Dorman (1992a) and VandenBerg (1983, 1992). Mass loss has been incorporated into the code for stars with convective envelopes—the mass of the convective envelope is reduced by an amount given by a specified mass-loss-law at each timestep. A new internal mass mesh grid is created for each model because of the reduced surface mass. Upon convergence of the stellar structure equations, a valid stellar model of reduced mass is obtained.

We neglect mass loss along the main sequence. For our evolutionary tracks we assume that mass loss takes place only during the red giant branch phase. The mass loss prescription that we use here is the widely used Reimers Formula (Reimers 1975, 1977):

$$\dot{M} = -4 \times 10^{-13} \eta_R \frac{L}{gR} M_{\odot} \text{ yr}^{-1}$$

where η_R is a mass loss efficiency parameter, L is the luminosity, g is the surface gravity, and R is the radius, with L , g , and R in solar units. To produce a “normal” globular cluster horizontal branch requires $\eta_R \sim 0.25 - 0.5$ (Renzini 1981).

If the mass loss rate is large enough, the star leaves the RGB before reaching the tip. It evolves toward higher temperatures at constant luminosity after RGB peel-off. This results in a decrease in radius and an increase in surface gravity, which should cause the mass loss rate to decrease. For hot stars, different mass loss mechanisms may be important (Chiosi & Maeder 1986), but the mass loss rates are expected to be significantly smaller in the tightly bound remnants of low mass stars than in young massive stars in which high temperature winds have been observed and modeled. In anticipation of this physically expected decrease in mass loss rate, we turn off the mass loss after the convective envelope contains less than $10^{-3} M_{\odot}$.

The code STEV calculates stellar models using the Eggleton non-Lagrangian scheme (Eggleton 1971) for the conventional red giant branch evolution (VandenBerg 1992), and a standard Lagrangian grid for all other evolutionary phases. The non-Lagrangian scheme was designed primarily for the evolution of stars with a thin burning shell, as an alternative to the shell-shifting technique (see Sweigart & Gross 1978). It provides a faster means of computing the evolution when there is a rapidly advancing shell, since it does not require that the timestep be small enough to ensure that only a small mass fraction of the burning shell is consumed between models. Typical RGB calculations require about 600 models, a third of which are used to compute small timesteps close to the He-flash. However, since our implementation of the Eggleton scheme provides only limited capability for following a detailed nuclear reaction network (but see Han, Podsiadlowski, & Eggleton 1995), the calculations are halted after the star leaves the RGB, and continued with the Lagrangian code, which follows 7 elements in a fully implicit scheme. The non-Lagrangian scheme computes the H, He and ^{14}N profiles, but is able to follow the evolution of the other elements in a separate calculation, for use at the transition. The conversion from one evolutionary scheme into another does not affect the qualitative behavior of the models.

The surface boundary condition is computed differently for the three sub-solar metallicities and the other two metallicities. The code has the option of using surface pressures derived from computed model atmospheres (VandenBerg & Bell 1985) or assuming a T - τ (temperature stratification) relation. Since the

model atmospheres are available only in a restricted range in temperature, evolutionary tracks with wide variations in temperature and gravity cannot use the model grids for the entire evolution. We chose to use the model pressures for $[\text{Fe}/\text{H}] < 0$ until the tracks peeled off the RGB, after which we used the Lagrangian scheme and the Eddington approximation. The result is a gap in the evolutionary sequences in the more metal poor calculations at the transition point. For higher metallicity models the same procedure cannot be used since the pressure grids, where available, do not cover the range of surface values during the crucial period of rapid mass loss. In this case, the Eddington approximation was used from the ZAMS. The stellar models were converted from non-Lagrangian co-ordinates to Lagrangian co-ordinates at which point $M_{\text{env}} \approx 10^{-5} M_{\odot}$ after peel-off.

For tip-flashers evolution was continued until $L_{\text{He}} \geq 62.5 L_{\odot}$. In the case of the hot flashers and the flash-manqués the code ran until it was no longer able to continue the evolution. This occurred at $L_{\text{He}} \gtrsim 30 L_{\text{H-shell}}$ for the hot flashers. Instead of pursuing the lengthy computations required to go through the He flash, the stars were assumed to appear on a ZAHB with varying core mass. ZAHB models were created using the initialization procedure outlined in Dorman, Lee, & VandenBerg (1991), with the hydrogen shell composition profile being extracted from the last converged pre-flash model for each star. Since the stars which lose more mass have different (thinner) hydrogen burning shells, the relevant composition profile was found for each value of η_R for which the model underwent the helium flash.

2.2. RGB Evolution

We computed a number of RGB models with different values of Reimers’ η_R for $[\text{Fe}/\text{H}] = -2.26, -1.48, -0.78, 0.0$, and 0.37 . We chose the initial mass of the stars such that their MS ages were between 12.5 and 14.5 Gyr. Thus, in our discussion below we will be considering different stellar populations at roughly constant age. At each metallicity, we calculated RGB models for $\eta_R = 0.0, 0.3, 0.6$. We increased η_R in steps of 0.05 for $\eta_R > 0.6$ until there were at least two He-WD tracks for each metallicity. A summary of the calculations for all the metallicities is given in Table 1. All models of the same metallicity are grouped together, with the metallicity and initial stellar mass, M_{in} , indicated at the beginning of each group. The first column lists the values of η_R for which RGB models were created. The second and third columns contain the final mass, M_f , and the He-core mass, M_c , of the stars respectively. The final envelope masses, M_{env} , of the RGB models are given in the fourth column. The asterisks denote convective envelopes, the rest of the envelope masses being the difference between the core mass and the total stellar mass. The fifth column, titled “Remark”, indicates the evolutionary behavior of the models i.e. a star marked as “He-flasher” is a classic RGB tip flasher, while a remark of “RGB peel-off, He flasher” indicates a hot He-flasher, and “RGB peel-off, He WD” means that the star peeled-off the RGB and failed to ignite helium.

The HR diagram of the RGB tracks for the models listed in Table 1 are shown in Figure 1. The figure shows the evolution of the models from the ZAMS until helium flash or the He WD phase. All five metallicities are shown. The solid lines are the tracks of flashing models, the dotted ones are flash-manqué models. The location of the helium flash for stars that flash away from the RGB are indicated by open

TABLE 1
MODEL CALCULATIONS

η_R	$M_f (M_\odot)$	$M_c (M_\odot)$	$M_{env} (M_\odot)$	Remark
(a) $[\text{Fe}/\text{H}] = -2.26$; $M_{in} = 0.8M_\odot$				
0.00	0.8000	0.5005	0.2895*	He-flasher
0.30	0.7066	0.5003	0.1965*	He-flasher
0.60	0.5976	0.5006	0.0874*	He-flasher
0.65	0.5781	0.5006	0.0685*	He-flasher
0.70	0.5570	0.5007	0.0473*	He-flasher
0.75	0.5360	0.5006	0.0269*	He-flasher
0.80	0.5149	0.5007	0.0070*	RGB peel-off, He-flasher
0.85	0.5050	0.5000	0.0050	RGB peel-off, He-flasher
0.90	0.5006	0.4983	0.0023	RGB peel-off, He-flasher
0.95	0.4963	0.4945	0.0018	RGB peel-off, He-flasher
1.00	0.4924	0.4905	0.0019	RGB peel-off, He-flasher
1.05	0.4888	0.4869	0.0017	RGB peel-off, He-flasher
1.10	0.4851	0.4832	0.0019	RGB peel-off, He-flasher
1.15	0.4820	0.4800	0.0020	RGB peel-off, He WD
1.20	0.4788	0.4768	0.0020	RGB peel-off, He WD
(b) $[\text{Fe}/\text{H}] = -1.48$; $M_{in} = 0.8M_\odot$				
0.00	0.8000	0.4902	0.3098*	He-flasher
0.30	0.6853	0.4900	0.1882*	He-flasher
0.60	0.5453	0.4905	0.0548*	He-flasher
0.65	0.5200	0.4903	0.0239*	He-flasher
0.70	0.4958	0.4905	0.0008*	RGB peel-off, He-flasher
0.75	0.4904	0.4886	0.0018	RGB peel-off, He-flasher
0.80	0.4854	0.4840	0.0014	RGB peel-off, He-flasher
0.85	0.4807	0.4793	0.0014	RGB peel-off, He-flasher
0.90	0.4764	0.4750	0.0014	RGB peel-off, He-flasher
0.95	0.4724	0.4709	0.0014	RGB peel-off, He WD
1.00	0.4686	0.4672	0.0014	RGB peel-off, He WD
(c) $[\text{Fe}/\text{H}] = -0.78$; $M_{in} = 0.85M_\odot$				
0.00	0.8500	0.4817	0.3683*	He-flasher
0.30	0.7097	0.4815	0.2232*	He-flasher
0.60	0.5306	0.4819	0.0487*	He-flasher
0.65	0.4982	0.4816	0.0127*	RGB peel-off, He-flasher
0.70	0.4826	0.4809	0.0017	RGB peel-off, He-flasher
0.75	0.4771	0.4761	0.0010	RGB peel-off, He-flasher
0.80	0.4720	0.4709	0.0011	RGB peel-off, He-flasher
0.85	0.4763	0.4662	0.0011	RGB peel-off, He-flasher
0.90	0.4629	0.4618	0.0011	RGB peel-off, He WD
0.95	0.4588	0.4577	0.0011	RGB peel-off, He WD
1.00	0.4550	0.4538	0.0012	RGB peel-off, He WD
(d) $[\text{Fe}/\text{H}] = 0.0$; $M_{in} = 0.95M_\odot$				
0.00	0.9500	0.4701	0.4766*	He-flasher
0.30	0.7723	0.4702	0.2987*	He-flasher
0.60	0.5234	0.4702	0.0505*	He-flasher
0.65	0.4781	0.4702	0.0053*	RGB peel-off, He-flasher
0.70	0.4687	0.4679	0.0008	RGB peel-off, He-flasher
0.75	0.4634	0.4625	0.0009	RGB peel-off, He-flasher
0.80	0.4582	0.4574	0.0008	RGB peel-off, He-flasher
0.85	0.4540	0.4531	0.0009	RGB peel-off, He-flasher
0.90	0.4495	0.4487	0.0008	RGB peel-off, He WD
0.95	0.4455	0.4447	0.0008	RGB peel-off, He WD

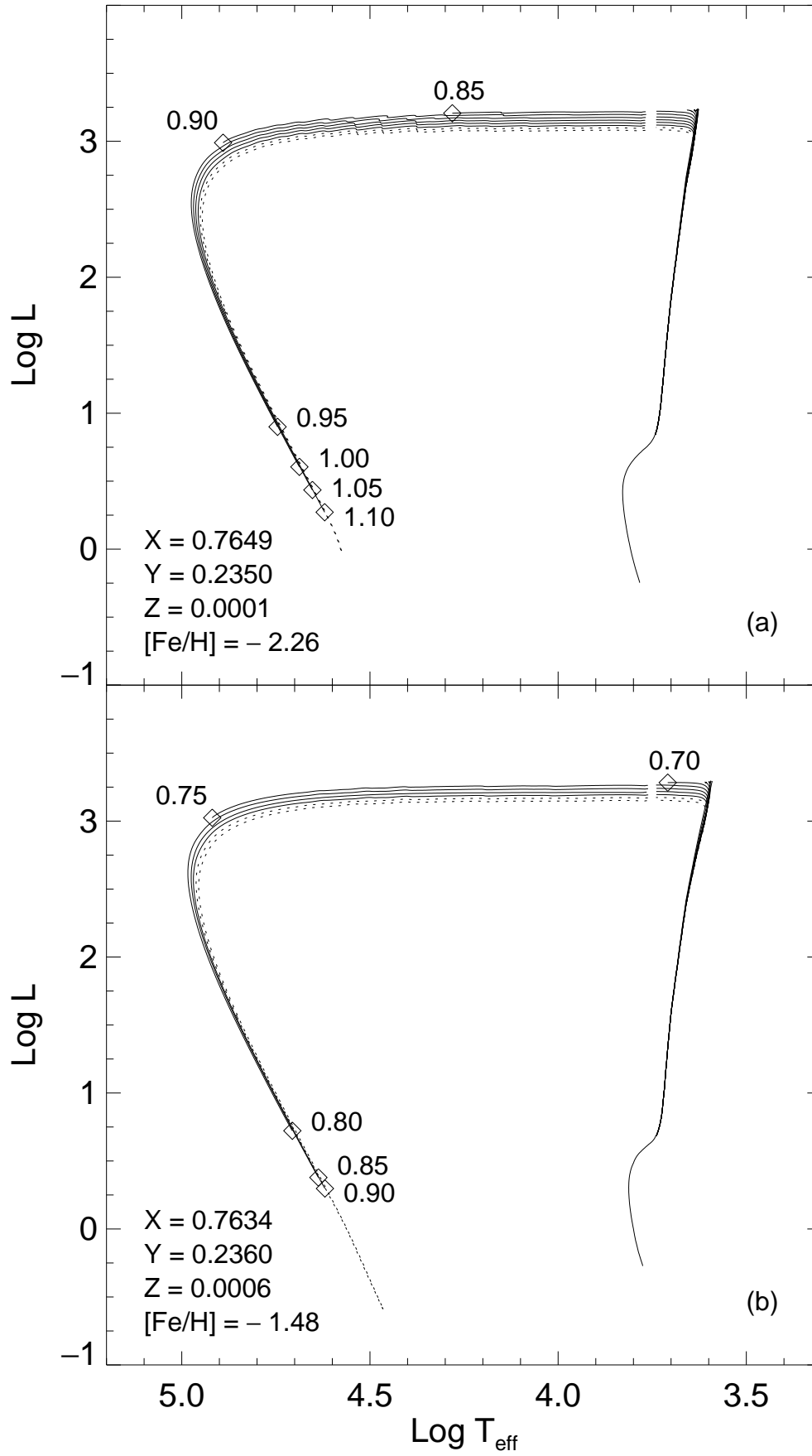
TABLE 1—*Continued*

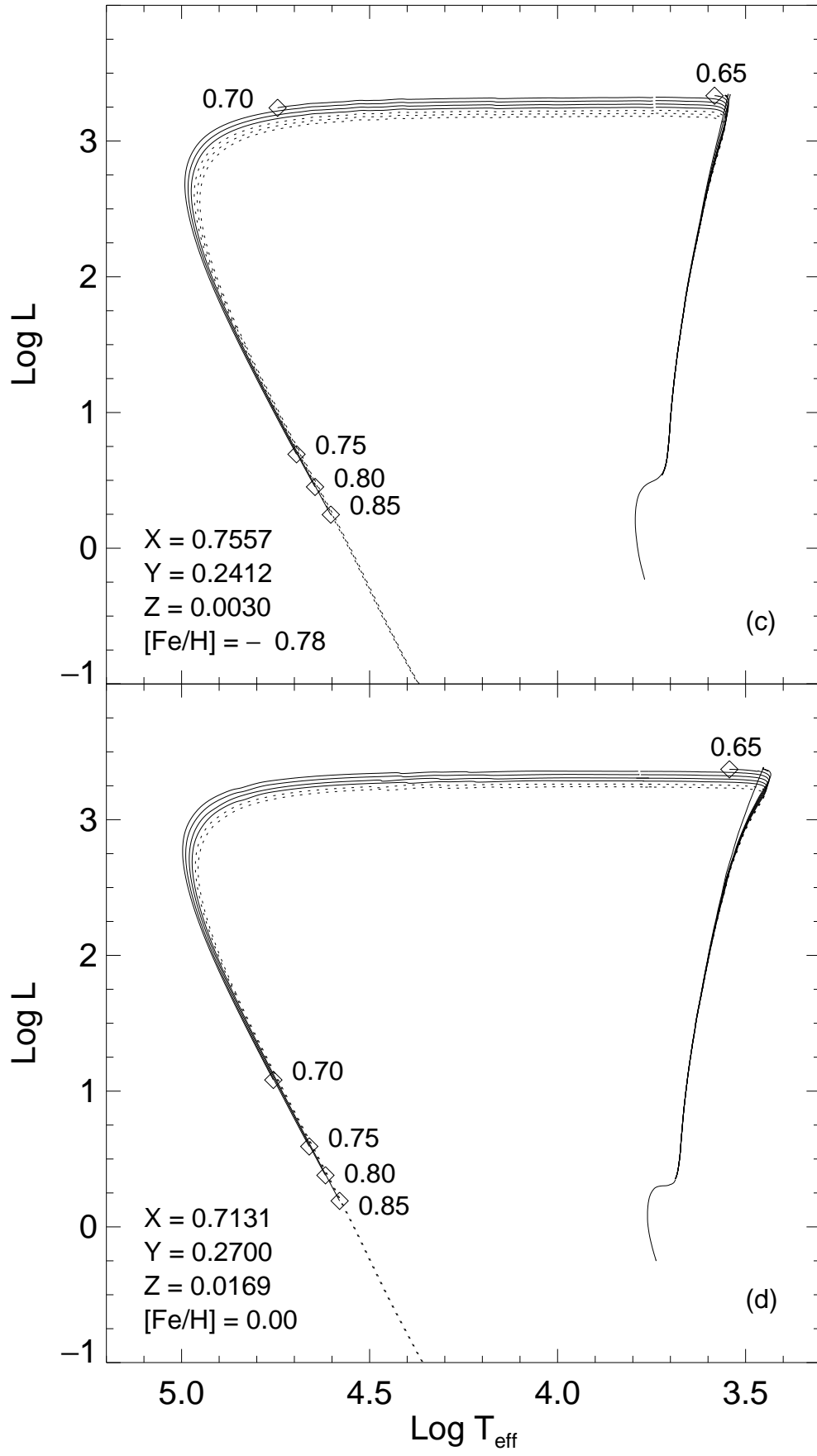
η_R	$M_f (M_\odot)$	$M_c (M_\odot)$	$M_{env} (M_\odot)$	Remark
(e) $[\text{Fe}/\text{H}] = 0.37$; $M_{in} = 1.08 M_\odot$				
0.00	1.0800	0.4642	0.6132*	He-flasher
0.30	0.9097	0.4644	0.4427*	He-flasher
0.60	0.6749	0.4644	0.2079*	He-flasher
0.65	0.6244	0.4643	0.1576*	He-flasher
0.70	0.5699	0.4643	0.1033*	He-flasher
0.75	0.5140	0.4643	0.0476*	He-flasher
0.80	0.4672	0.4643	0.0110*	RGB peel-off, He-flasher
0.85	0.4625	0.4616	0.0009	RGB peel-off, He-flasher
0.90	0.4582	0.4574	0.0008	RGB peel-off, He-flasher
0.95	0.4541	0.4534	0.0007	RGB peel-off, He-flasher
1.00	0.4503	0.4496	0.0007	RGB peel-off, He-flasher
1.05	0.4468	0.4461	0.0007	RGB peel-off, He WD
1.10	0.4434	0.4427	0.0007	RGB peel-off, He WD

NOTE.— M_{in} is the initial mass of the star, M_f is the final mass of the star after mass loss, M_c is the Helium core mass of the star either when the helium flash takes place or at the end of the track for the stars that form He White dwarfs. M_{env} is the envelope mass, the asterisks denote convective envelopes. The “Remark” column indicates the evolutionary behavior that results from RGB mass loss.

diamonds and have the corresponding η_R value listed next to them. The break in the peel-off tracks is where the conversion from non-Lagrangian to Lagrangian co-ordinates takes place. We see from Figure 1 and Table 1 that there is a range of masses for which models peel-off the RGB but still undergo the helium flash for all metallicities. The hot-flash behavior occurs for values of η_R 2–3 times larger than that required to produce normal HB stars. Contrary to our initial expectations, hot-flash behavior occurs for a fairly large range of η_R . Some of the peel-off stars show weak hydrogen shell flashes while moving from the RGB to the cooling curve. This is most clearly seen in the $[\text{Fe}/\text{H}] = -2.26$ tracks in Figure 1(a). Whether these flashes are numerical or due to a real instability is not known. The models of CC93 do not show similar flashes.

None of our low metallicity models have enhanced oxygen. Enhancement of oxygen and other α -nuclei elements is often found in metal poor stars (see Wheeler et al. 1989 for a review). Increasing oxygen affects RGB evolution in two ways: the rate of evolution is sped up (at a given luminosity) and the flash occurs at higher luminosity. The track in the HR diagram is essentially unshifted, because the opacity at low T is dominated by other elements (Renzini 1977). Because of the faster evolution the core mass at flash is smaller. As far as mass loss goes there are compensating factors: there is less time to lose mass as the evolution is faster, but the evolution to higher L increases mass loss. We performed one comparison case with $[\text{Fe}/\text{H}] = -2.26$, $[\text{O}/\text{Fe}] = 0.0, 0.75$ and $\eta_R = 0.0, 0.95$. As expected the oxygen enhanced models have smaller core masses for both η_R values and the flash occurs at higher L for the $\eta_R = 0.0$ case. For $\eta_R = 0.95$, more mass was lost and the star peels off at higher L compared to the $[\text{O}/\text{Fe}] = 0$ case. Since our results suggest no change in qualitative behavior with total metallicity we expect the effect of enhanced O to be small.





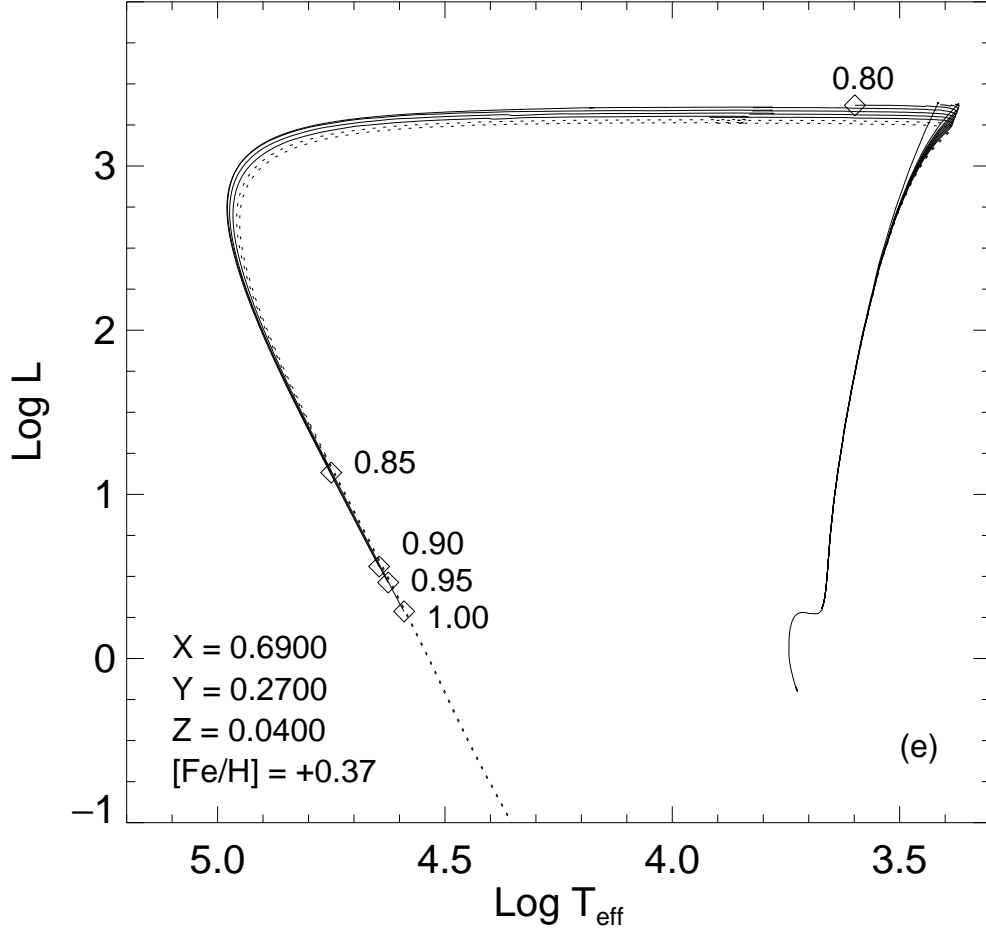


Fig. 1.— HR Diagram of the red giant branch evolutionary tracks with mass loss for the metallicities considered— $[Fe/H] = -2.26, -1.48, -0.78, 0.0, 0.37$. The hydrogen abundance, X , the helium abundance, Y , the heavy element abundance, Z , and the metallicity, $[Fe/H]$ are shown for each panel. The solid lines are tracks which end with a helium flash. For the RGB peel-off stars the location of the helium flash is indicated by an open diamond and the corresponding η_R value is listed next to the symbol. These stars are the “Hot - He flashers.” The dotted lines are tracks which form He White Dwarfs. The break in the peel-off tracks is where the conversion from non-Lagrangian to Lagrangian evolutionary schemes takes place. Table 1 details the model parameters.

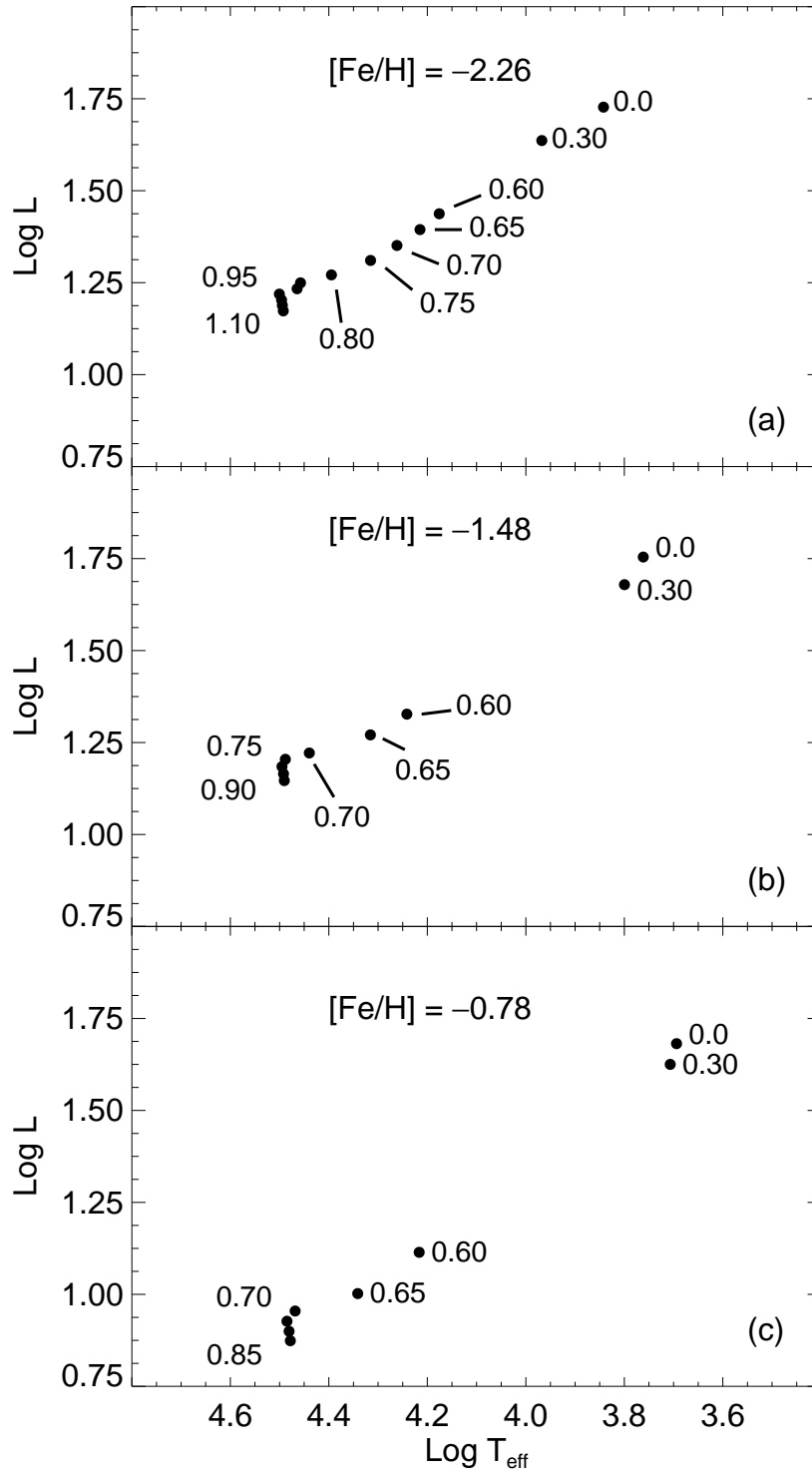
As noted earlier, the mass loss was terminated when the envelope mass becomes less than $10^{-3} M_{\odot}$. To see whether this assumption affects the hot-flash behavior, we also computed a track in which the mass loss was allowed to continue until the envelope mass was so small that it would be entirely removed within a timestep. The core mass of the star in this case changed by $10^{-3} M_{\odot}$, which is of the order of the numerical uncertainty in determining the core mass at the He-flash. This again suggests that the arbitrariness of the point at which mass loss was terminated does not change the qualitative behavior of the models.

One particularly important result to realize here is that the M_c for the hot-flashers is smaller than the (more or less) constant value for the tip-flashers and that it decreases as η_R increases. It is commonly believed that the rising temperatures in the He core are due to the march of the hydrogen burning shell through the star. Our results show that the core temperatures rise because of the contraction of the core, and that contraction continues whether or not the mass of the core is increasing. We find that any star which has a surviving H-envelope when its He core is within $0.015\text{--}0.018 M_{\odot}$ of M_{fl} , the classical core mass at flash, will undergo a He flash. On the RGB near the flash $L \sim M_c^5$, so any star which gets to within ~ 0.4 mag of the tip luminosity will flash either at the tip or as a hot-flasher. *Hence any mass loss law that produces a substantial fraction of the total mass lost in the upper ~ 0.4 mag of the RGB has the potential to produce a substantial population of hot-flashers.* This result, as well as that of Castellani et al. (1995) implies that there is no minimum envelope mass for the HB. This finding contradicts the assumption of Yi et al. (1995) that He burning cannot be initiated for $M_{\text{env}} \leq 0.02 M_{\odot}$. Yi et al. (1995) seem to have based their assumption on the work of Sweigart, Mengel, & Demarque (1974), who used a plausibility argument to suggest that the probability of having HB stars with $M_{\text{env}} \leq 0.02 M_{\odot}$ is small.

The peel-off stars will be indistinguishable from P-EAGB stars as they evolve to the cooling curve before the helium flash. Their luminosity ($L \gtrsim 1000 L_{\odot}$) and evolutionary timescale when crossing the HR diagram (1–2 Myr) are similar. Both types of objects would be rare in populations as small as globular clusters because of the brevity of this crossing phase. In a cluster containing 10^3 RGB stars brighter than the HB and with lifetimes of 10^8 yr, one would expect to find $\sim 10 f_{\text{peel-off}}$ peel-off stars, where $f_{\text{peel-off}}$ is the fraction of RGB stars that peel-off the RGB. The value of $f_{\text{peel-off}}$ must be less than the fraction $N(\text{EHB})/N(\text{HB})$. The globular cluster ω Cen contains the largest fraction of EHB stars at roughly 20% [DOR95]. For this cluster one would expect to have one or no RGB peel-off stars. This is consistent with the number of stars predicted to exist at this luminosity. Since these stars are so rare and are similar to P-EAGB stars, it would be very difficult to verify their existence as such in the Galactic field or in integrated light.

2.3. Zero-Age Horizontal Branch Models and post-RGB evolution

ZAHB models for each composition are shown in Figure 2. The hot-flashers do not follow the classical ZAHB as defined by Iben & Rood (1970) which is a constant core mass sequence. Their helium core mass is less than that of the normal ZAHB models. These stars have very small envelopes and hence will be very blue, and slightly less luminous than the regular ZAHB. They form a “blue hook” at the blue end of the ZAHB as can be seen in Figure 2. The blue hook stars are a part of the EHB population and have almost



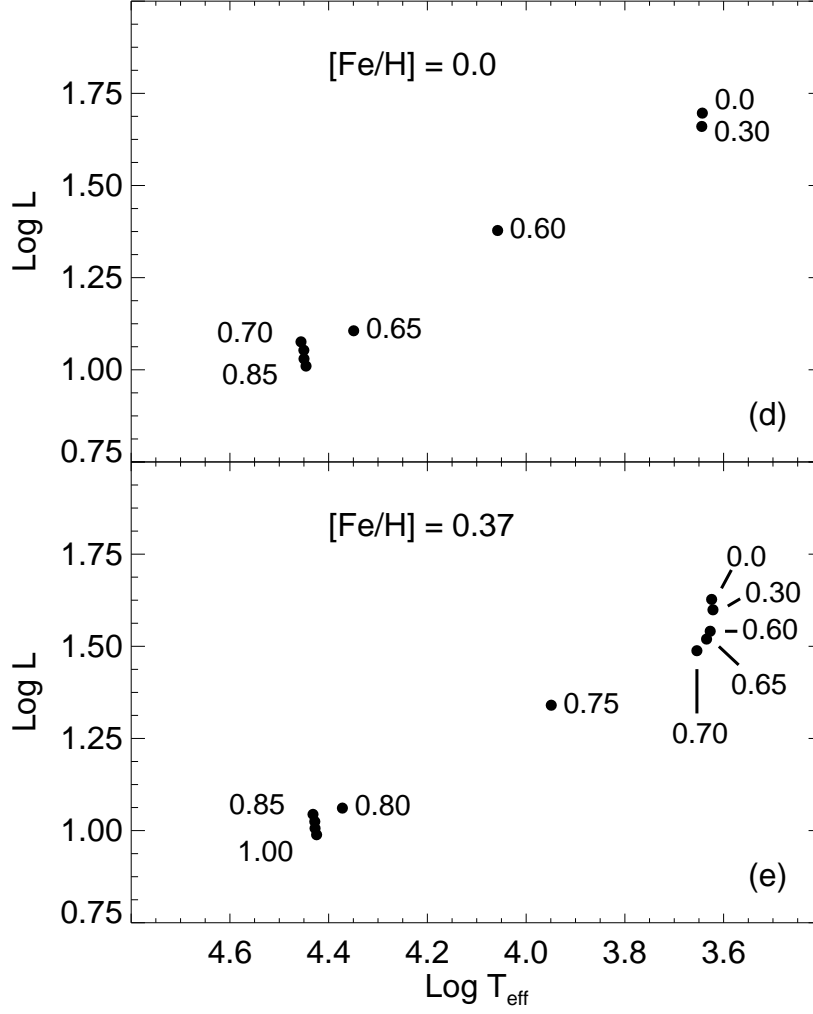


Fig. 2.— The HR diagram of ZAHB models corresponding to the flashing RGB models from Figure 1 are shown for all five metallicities. The corresponding η_R values are marked. The hot He-flashers form a blue hook at the blue end of the ZAHB at all metallicities.

the same envelope masses but different helium core masses. Therefore they form a sequence that is fairly constant in temperature but has a spread in luminosity. The temperature spread is $\leq 750K$. The length of the hook can be estimated using $L \sim L_{\text{He}} \sim M_{\text{core}}^3$ to be ~ 0.1 mag. The blue hook sequence is cooler by $\Delta \log T_{\text{eff}} \sim 0.1$ than the helium main sequence (Castellani et al. 1995).

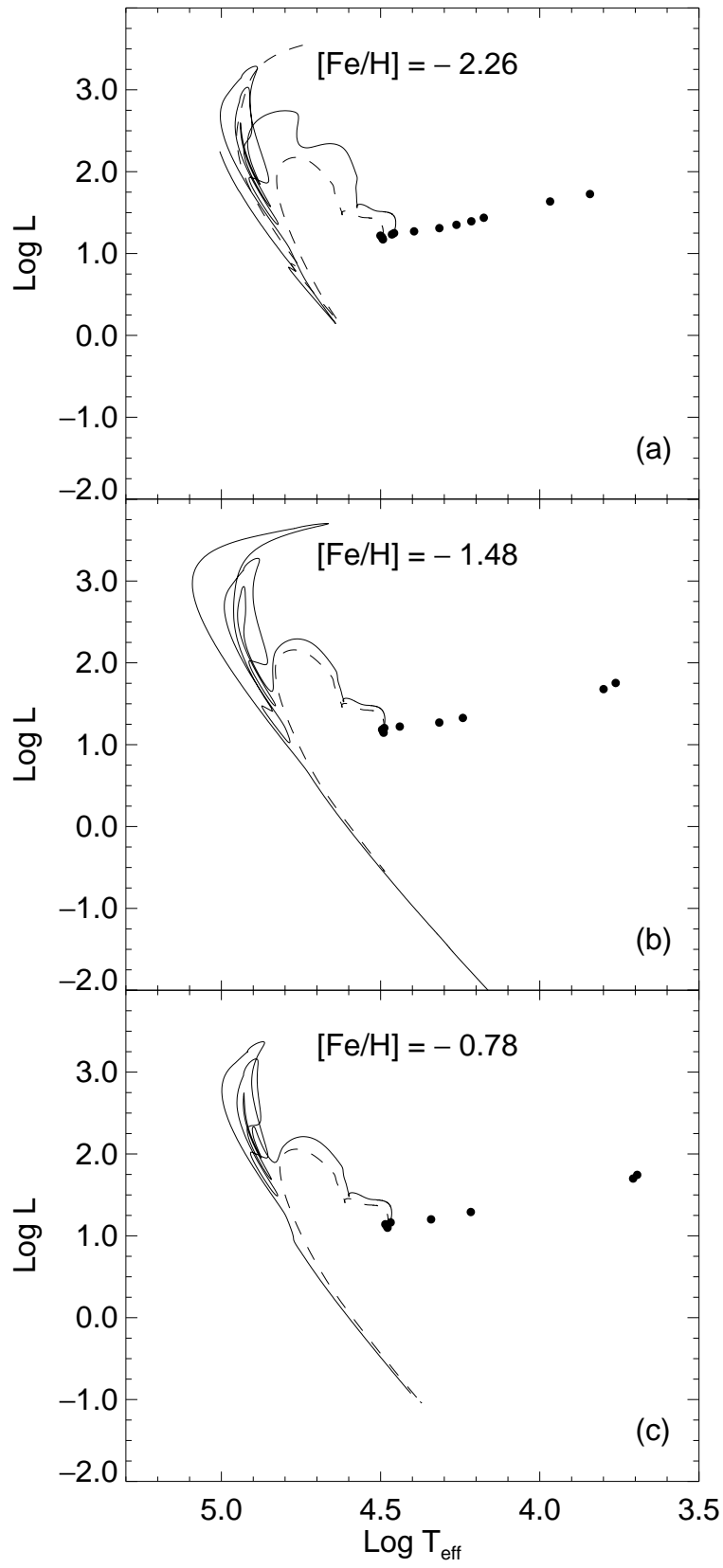
Blue-hook stars will evolve into AGB-manqué objects with similar behavior to that of the lowest mass “traditional” ZAHB models of DRO93. Both the blue-hook EHB stars and their AGB-manqué progeny will emit considerable UV radiation. We computed the post-RGB evolution of two such models for each metallicity. The two models that were followed had $\eta_R = \eta_R(\text{flash})$ and $\eta_R(\text{peel-off}) + 0.05$, where $\eta_R(\text{flash})$ is the highest value of η_R for which a helium flash occurs and $\eta_R(\text{peel-off})$ corresponds to the transition between classic red giant tip flashers and hot He-flashers. The rest of the ZAHB stars are expected to evolve as normal (see DRO93). Figure 3 shows the post-RGB evolutionary tracks of the two blue hook stars whose evolution we computed. For the initial vertical part of the tracks (~ 1 mag), evolution is relatively slow and accounts for about 80% of the post-RGB life time. An ensemble of blue-hook stars will form an almost vertical band of hot HB stars which starts about 0.1 magnitudes below the ZAHB with $\sim 80\%$ of the stars lying within about one magnitude above it. With some imagination one can see such a sequence in the hot HB stars observed in ω Cen (Fig. 10 of Whitney et al. 1994).

3. DISCUSSION

Our use of Reimers’ formula as a mass loss prescription could be questioned. This formula has no physical basis and was constructed on the basis of observation and dimensional analysis. There are alternate ways of parametrizing mass loss, none of which have been found to be exceptionally better or worse than Reimers’ formula (see Dupree 1986; Chiosi & Maeder 1986). Ideally, one would like to use a mass loss rate that is derived from a mass loss mechanism believed to operate in cool giants. Unfortunately the exact mechanism that drives mass loss is not known; the gross stellar parameters (temperature, luminosity, gravity, metallicity) are obviously insufficient to determine the mass loss uniquely. Instead, the inferred spread in total mass lost may somehow be tied to individual properties such as rotation rates (Fusi Pecci & Renzini 1978) and magnetic field strengths, and may be related to the abundance variations detected in globular cluster stars (see Kraft 1994 for a review).

As for possible physical mechanisms for mass loss, thermally driven winds, wave-driven winds, radiation pressure on molecules and/or dust grains, and winds resulting from shock waves are those most widely cited (see Holzer & MacGregor 1985 for a review). It is possible that more than one mechanism operates in a single star simultaneously. For the Sun, it is now believed that the effects of rotation and convection lead to the magneto-hydrodynamic heating of the solar corona, which gives rise to the solar wind (Spruit, Nordlund, & Tittle 1990).

Observations of cool, low-gravity stars show that the outflowing material is moving with asymptotic velocities that are considerably lower than the escape velocity of the star. Therefore, only a small fraction of the energy that is added to the stellar atmosphere for the purpose of fueling the wind is used to lift the



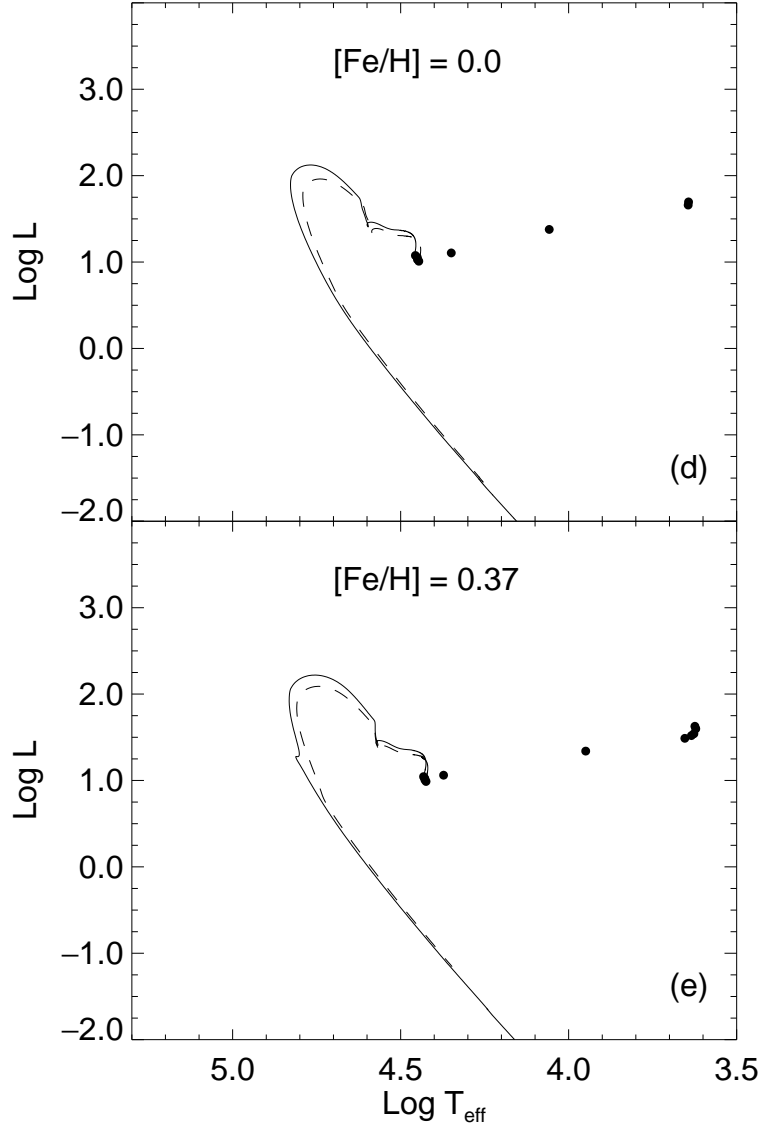


Fig. 3.— The ZAHB Models are shown in this figure with two AGB-manqué tracks for all metallicities. The AGB-manqué tracks are for two stars in the blue hook as indicated in the text.

wind out of the gravitational field of the star. From the low asymptotic velocities one can actually expect to learn very little about the mechanism driving the mass loss since we observe only a small part of the driving energy (Holzer & MacGregor 1985). The electron temperatures in cool supergiants are found to be around 10^4 K as opposed to 10^6 K for the solar corona, which rules out thermally driven winds (Dupree 1986). Large rates of mass loss also imply that the mass loss mechanism is fairly efficient close to the stellar surface where the densities are relatively high, which in turn places a constraint on the temperature at which the mechanism operates.

Observations show that mass loss rates increase with decreasing surface gravity and increasing stellar luminosity. The mass loss rates themselves are uncertain in some cases to a factor of 5 or even 10. Obtaining mass loss rates is a complex process and only a few stars have well determined mass loss rates. The spectral lines (Ca H & K, $H\alpha$, etc) used to study mass loss originate at different depths in the stellar atmosphere. Hence a better understanding of the atmospheric structure and the origin of the lines is necessary. In the face of our ignorance on this crucial matter, the Reimers formula seems as good a parametrization as any, in that it obeys the observed functional dependences and is dimensionally correct.

The conclusions we draw depend mainly on the escalation of the assumed mass loss rate close to the RGB tip. Our generic results for core He burning and beyond should still hold if mass loss rates increase close to the RGB tip at least as sharply as in the Reimers formula. Using the Reimers formula or any other formulation which depends only on surface parameters, mass loss continues until the star peels off the RGB. These stars undergo He ignition so long as peel-off occurs sufficiently near (~ 0.4 mag) the RGB-tip. The helium cores are slightly smaller than those produced in RGB tip-flashers, and the ensuing evolution is the hot-flash/blue-hook behavior described here. We anticipate that a physically motivated mass loss law will almost certainly depend on the global properties of the convective zone. In reality mass loss may stop as the convective envelope approaches some minimum size $M_{\text{ce,min}}$. After mass loss is terminated M_{env} will continue to decrease as the H burning shell advances. These stars will still ignite He if the mass loss is turned off within ~ 0.4 mag of the tip. Depending on the circumstances, He ignition could be on the RGB or in a hotter phase. The core He burning stars resulting from these stars would have envelopes ranging from our small values up to $M_{\text{ce,min}}$. The blue-hook will be smeared in $\log T_{\text{eff}}$. Indeed, the observed degree of smearing of EHB stars can give a clue to the mass loss mechanism.

The “standard model” of the HB requires that individual RGB stars arrive on the ZAHB with a distribution $P(M_{\text{ZAHB}})$ of masses (Rood 1973). This distribution together with the metallicity gives rise to the different HB morphologies observed in globular clusters. The distribution has typically been modeled by a gaussian truncated in some way to account for physical limits to the mass (Rood 1973)³. *There was no physical basis for selecting the form of $P(M_{\text{ZAHB}})$ used*, other than that it seemed to work and that random variables often tend toward being gaussian (i.e. the Central Limit Theorem). Indeed there are some counter examples where this kind of formalism fails (e.g., Rood et al. 1993; Liebert et al. 1994). The accuracy of the assumption is hard to assess since existing data do not allow us to distinguish easily between different intrinsic mass distributions. Below we consider the ZAHB population to be driven by a function of $P(\eta_R)$

³There are subtle differences in the truncation schemes of the various workers which could affect extremes like EHB populations.

instead of $P(M_{\text{ZAHB}})$. As far as matching globular cluster HBs, the HB mass depends almost linearly on η_R over most of the HB for appropriate compositions. Thus any distribution in M_{ZAHB} can be mapped into a distribution in η_R . In this scheme, the star-to-star variation in η_R is a way of modeling the effects of individual differences among stars that cause the mass dispersion. One might think of the parameter $\eta_R = \eta_R[\alpha(\mathbf{X})]$, for some α , which is a set of functions of all the physical variables \mathbf{X} on which mass loss rates do actually depend. In this way, α gives a mapping between the true dependence of mass loss (including stochastic effects) and the necessarily inadequate formulation we use here. For example, the distribution $P(\eta_R)$ might arise from a stochastic distribution in rotation rates, $\mathcal{P}(\omega)$. Even though we consider only simple distributions for $P(\eta_R)$ we recognize that quite complex forms for $P(\eta_R)$ could arise from a simple gaussian $\mathcal{P}(\omega)$. Indeed, smooth variations in quantities like rotation and magnetic fields often lead to bifurcated outcomes.

We now will use our results to consider how the frequency of EHB stars, or more specifically blue-hook stars, might vary with the metallicity of a stellar population. We have plotted η_R vs [Fe/H] in Figure 4 for η_R values that correspond to various HB fiducial points. Using η_R as the quantity on which the distribution depends, we can crudely estimate how the ZAHB population changes with metallicity. We define $\eta_R(\text{RHB})$ to be the largest value of η_R that still produces red HB stars at the ZAHB. $\eta_R(\text{RR})$ is the value of η_R that marks the center of the RR Lyrae strip (approximately $\log T_{\text{eff}} = 3.85$); $\eta_R(10000 \text{ K})$ (the value of η_R that produces stars at 10,000 K) is roughly the hot end of the “horizontal” part of the HB. The transition between the traditional RGB tip-flashers and the hot-flashers is $\eta_R(\text{peel} - \text{off})$. The largest value of η_R that allows a helium flash is $\eta_R(\text{flash})$. The blue hook stars lie between $\eta_R(\text{peel} - \text{off})$ and $\eta_R(\text{flash})$, and the other EHB stars very approximately occupy the region from $\eta_R(\text{peel} - \text{off}) - 0.05$ to $\eta_R(\text{peel} - \text{off})$. The approximate red end of the EHB population, $\eta_R(\text{EHB})$ has been indicated with the dashed line in Figure 4. This is a very crude estimate of where the cool end of the EHB population should lie and was obtained by using the post-RGB tracks from DRO93.

There are a number of conclusions one can reach from this figure. Throughout bear in mind that there are some EHB stars in globular clusters, and in some, if not all, cases they originate from extreme mass loss evolution in single stars. For example, there are many EHB stars in ω Cen, a low density, unrelaxed cluster with few classical indications of stellar interactions such as blue stragglers (Bailyn et al. 1992). The EHB stars are not concentrated toward the center; thus even in an unfavorable environment for binary interactions, many such stars are formed (see DOR95 for a discussion of single vs binary origin of EHB stars).

In summary, note the following:

- At low metallicity the range of values of η_R which produces EHB stars is comparable in magnitude to that producing the normal HB. *Producing EHB stars requires no more fine tuning than producing ordinary HB stars in globular clusters.*
- Despite the fact that high metallicity stars must lose more mass to reach the EHB (for comparable age systems) they can achieve this larger mass loss with η_R values that are comparable to those needed for the low metallicity stars. Viewed in this way, it is no more difficult to produce EHB stars at high metallicity than at low, although the corresponding physical interpretation of this result is unclear.

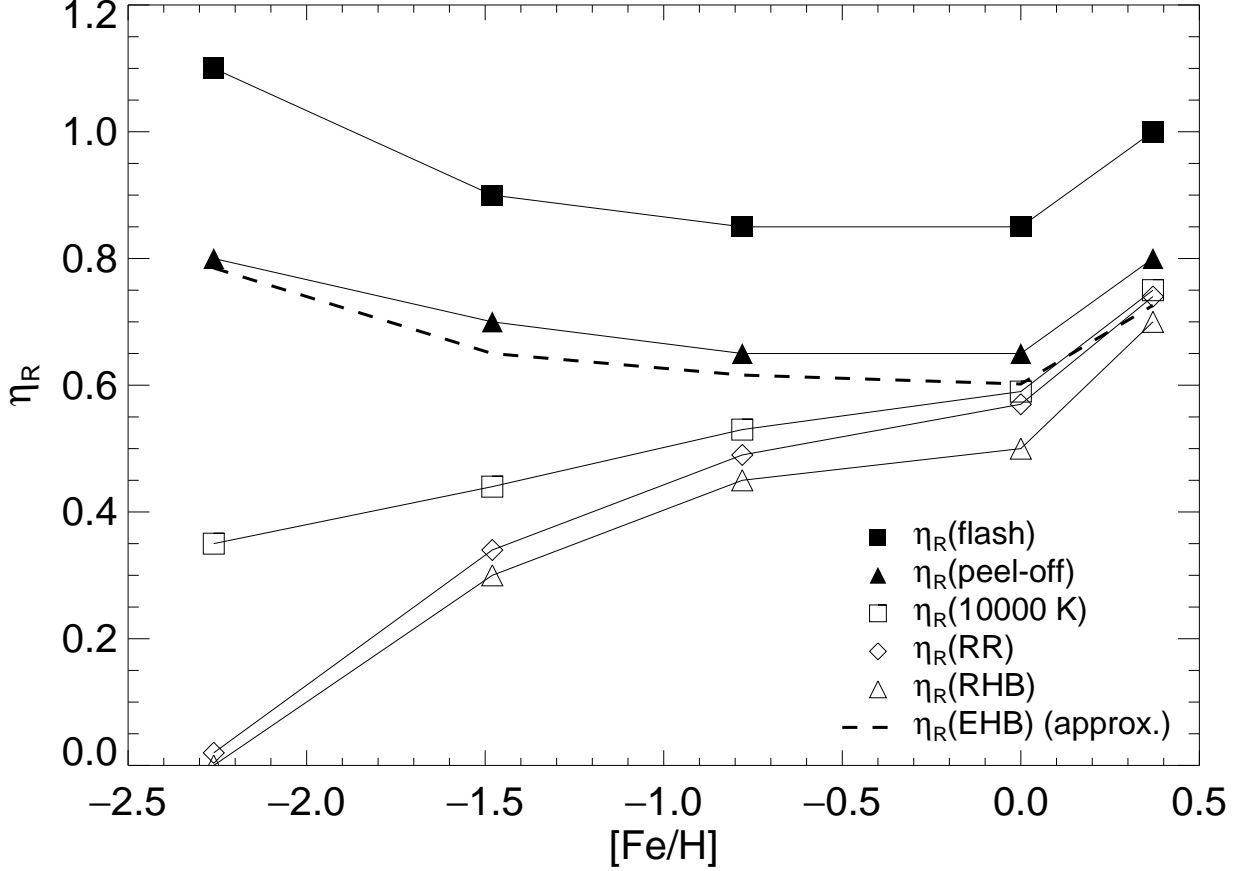


Fig. 4.— Plot of η_R vs Metallicity: The plot of η_R vs $[\text{Fe}/\text{H}]$ shows η_R that corresponds to (i) the blue end of RHB — $\eta_R(\text{RHB})$, (ii) RR Lyraes — $\eta_R(\text{RR})$, (iii) effective temperature of 10000 K — $\eta_R(10000 \text{ K})$, (iv) $\eta_R(\text{peel-off})$ — the transition between classic tip flashers and hot He flashers, (v) $\eta_R(\text{flash})$ — the largest value of η_R for which a flash occurs. The dashed line is the approximate location of $\eta_R(\text{EHB})$, the lowest value of η_R for which EHB stars form. The EHB stars very roughly occupy the region between $\eta_R(\text{EHB})$ and $\eta_R(\text{flash})$. Note the range of η_R corresponding to the mid-HB, $\eta_R(\text{RHB}) - \eta_R(10000 \text{ K})$, decreases as metallicity increases.

- The range of the mid-HB lies approximately from $\eta_R(\text{RHB})$ to $\eta_R(10000 \text{ K})$. Figure 4 shows that as metallicity increases, this range decreases. It becomes more difficult to make ordinary blue HB (IBHB) stars at higher metallicity—a point made by DOR95 but more explicitly demonstrated here. The ZAHB becomes increasingly bimodal for metal rich populations. This is consistent with observations of NGC 6791 which show a lack of IBHB stars and three sdB (EHB) stars (Liebert et al. 1994).
- The range of values of η_R producing EHB stars is almost constant for all metallicities. To make EHB stars at high metallicity, η_R does not have to increase and its distribution does not have to be more fine tuned.

3.1. Distribution of Stars on the ZAHB

Considering the ZAHB population distribution as a function of η_R instead of mass leads to a different perspective on the production of EHB stars. The ZAHB mass depends almost linearly on η_R till one get close to the blue hook. For the blue hook stars M_{ZAHB} does depend linearly on η_R but with a slope that is different from the rest of the ZAHB. The range in η_R for the blue hook is comparable to that of the rest of the ZAHB, but the range in mass of the blue hook stars is much smaller than the mass range of the ZAHB stars. Figure 4 shows that the EHB is made up of blue hook stars and slightly cooler extremely blue HB stars. The blue hook stars will contribute substantially to the EHB population if the *support* of $P(\eta_R)$ (the range of η_R where $P(\eta_R) \neq 0$) is sufficiently great. Therefore modeling the distribution of the ZAHB as a function of η_R ensures a reasonably well populated EHB. This circumstance arises jointly from the rapid increase in M_c and the escalation of the mass loss rate close to the RGB tip. In some sense, ZAHB models constructed with a $P(\eta_R)$ are more directly related to the underlying physics of mass loss than those using $P(M_{\text{ZAHB}})$, since the star “sees” mass loss rates, rather than “knows” its final ZAHB location.

Figure 5 shows the relationship between η_R and $\log T_{\text{eff}}$ of the ZAHB stars for the five metallicities used in this paper. The slope, $d\eta_R/d\log T_{\text{eff}}$, is larger at the blue and red ends of the ZAHBs. The slope of the mid-HB region is seen to decrease as metallicity increases. This is more clearly shown in Figure 5(f) where all the curves are superposed on each other. If the slope of these curves is an indication of the number of stars present at a given effective temperature on the ZAHB then it can be used to describe the ZAHB distribution to first order. The number of stars per $\log T_{\text{eff}}$ interval, $N(\log T_{\text{eff}}, \log T_{\text{eff}} + d\log T_{\text{eff}})$, will be given by

$$N(\log T_{\text{eff}}, \log T_{\text{eff}} + d\log T_{\text{eff}}) = P(\eta_R) \frac{d\eta_R}{d\log T_{\text{eff}}}.$$

The normalized slope of these curves is shown in Figure 6. Note that these curves are not smooth because of the discreteness of the numerical data used to construct them. The derivatives at the ends are very large. Hence the contrast between the ends and the mid-HB portion is increased relative to anything which could be observed. Both observational error and the binning required in a differential distribution function will

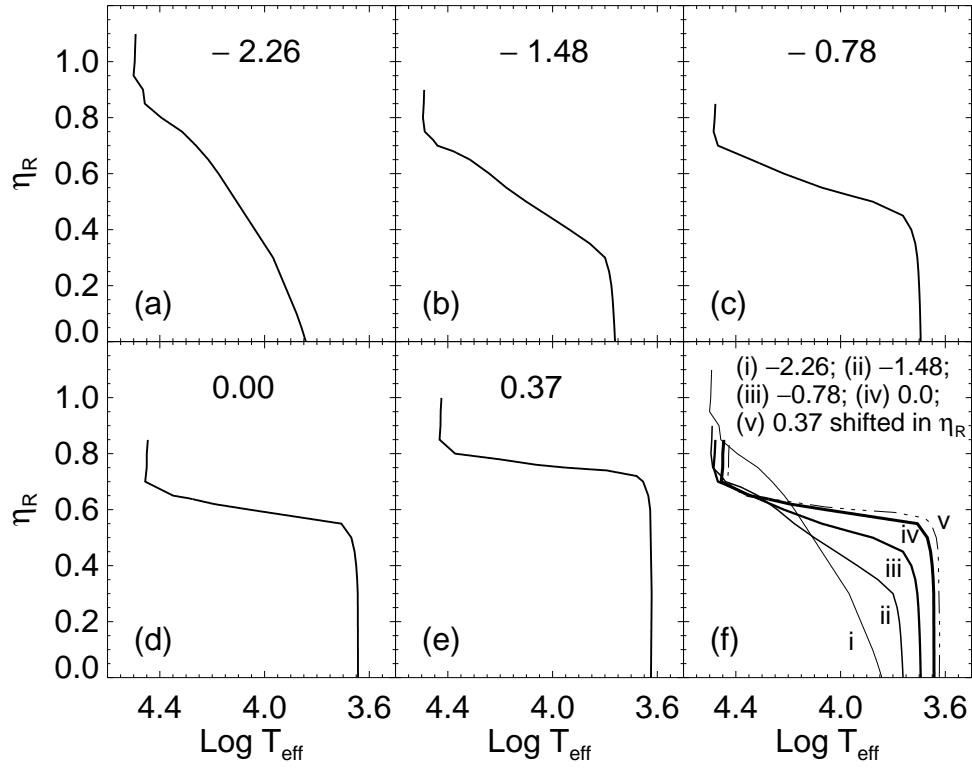


Fig. 5.— Plot of η_R vs $\log T_{\text{eff}}$ for the ZAHB stars plotted in Figure 2. The metallicity is indicated at the top of each panel for panels (a) to (e). Panel (f) shows all the plots for comparison with the $[\text{Fe}/\text{H}] = 0.37$ plot shifted down by 0.15 in η_R for clarity.

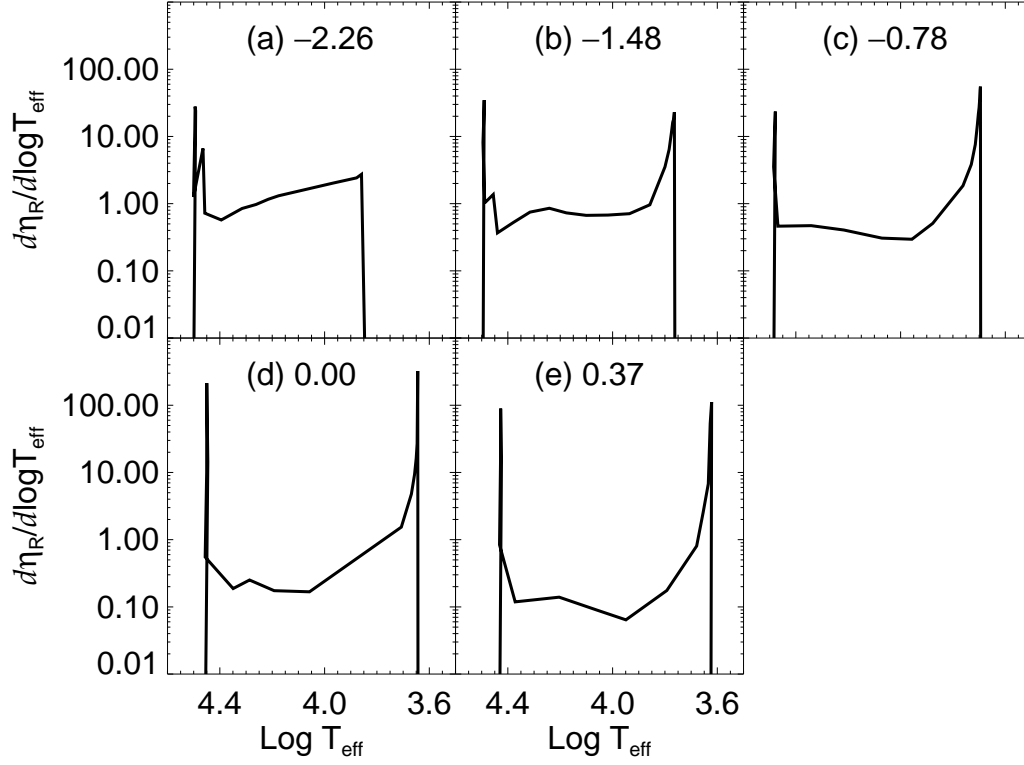


Fig. 6.— Plot of the slope, $d\eta_R/d\log T_{\text{eff}}$, of the curves in Figure 5 vs $\log T_{\text{eff}}$. The slope is directly related to the distribution of stars on the ZAHB for equally probable η_R . This is seen by comparing this figure and Figure 7. Note that these curves are not smooth because of the discreteness of the data. The derivatives at the ends are very large, hence the contrast between the ends and the mid-HB portion is increased relative to the binned distribution shown in Figure 7. The metallicity is indicated at the top of each panel.

smooth the ends. Figure 7 shows the effective temperature distribution of a thousand ZAHB stars resulting from a flat distribution in η_R i.e. $P(\eta_R) = \text{constant}$. The flat distribution of a thousand stars illustrated is created by linear interpolation of the ZAHB models computed from the flashing RGB stars. One can see that the curves in Figure 7 compare well with those in Figure 6.

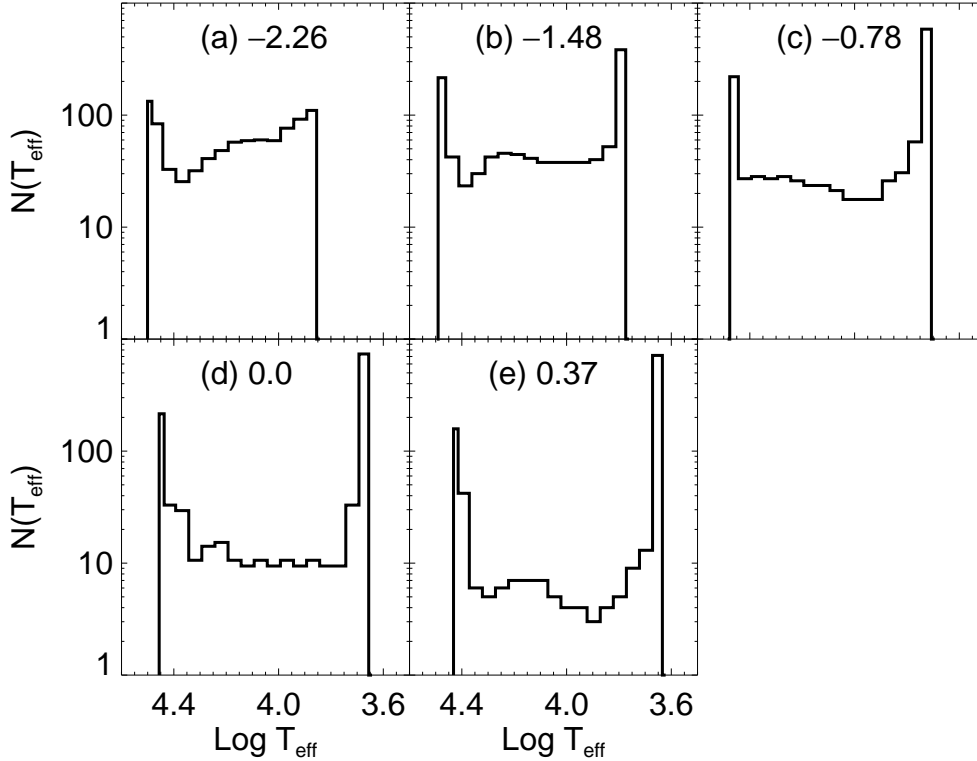


Fig. 7.— The effective temperature histogram of a thousand ZAHB stars. The metallicity is indicated at the top of each panel. The data are binned at intervals of 0.05 in $\log T_{\text{eff}}$. Note that these are log plots, so the decrease in the number of mid-HB stars with increasing metallicity appears somewhat exaggerated.

Using $P(\eta_R)$, both RHB and EHB stars can be produced if $P(\eta_R) \neq 0$ in the appropriate range. When cast as a “final” mass distribution $P(M_{\text{ZAHB}})$ it appears that fine tuning is required, but when $P(\eta_R)$ is used, it becomes clear that a fairly wide range of mass loss behavior produces EHB stars. However, for the metal rich populations, fine tuning is necessary to populate the mid-HB region. The bimodal nature of the metal rich ZAHBs arises both from the increased opacity of the metal rich stars and the increased importance of the H (via CNO cycle) burning shell. The envelopes of EHB stars are so small that shell burning is negligible and the opacity changes the temperature without affecting the structure (Dorman 1992b). The temperature

of the RHB is basically determined by the position of the Hayashi line (fully convective stars). As metallicity increases, both the opacity and H shell burning “push” stars from the mid-HB toward the Hayashi line, thus depopulating the mid-HB.

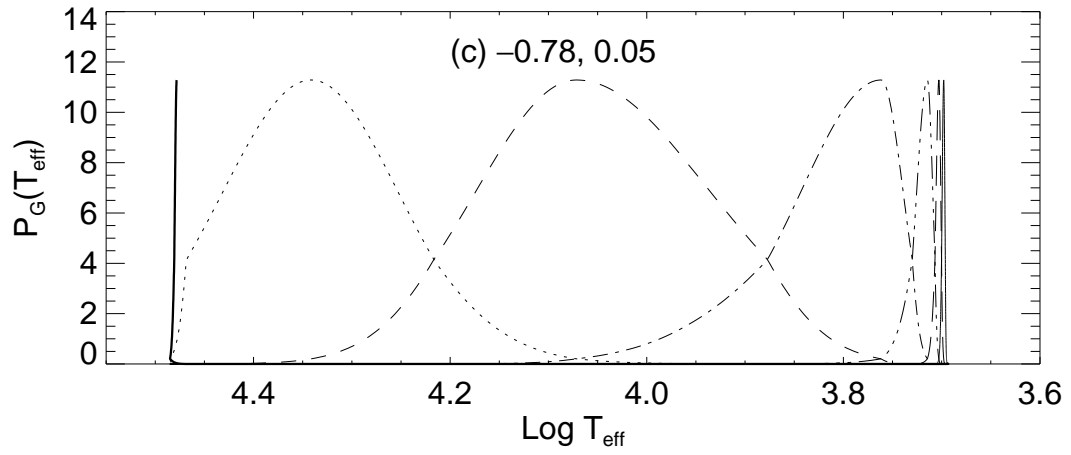
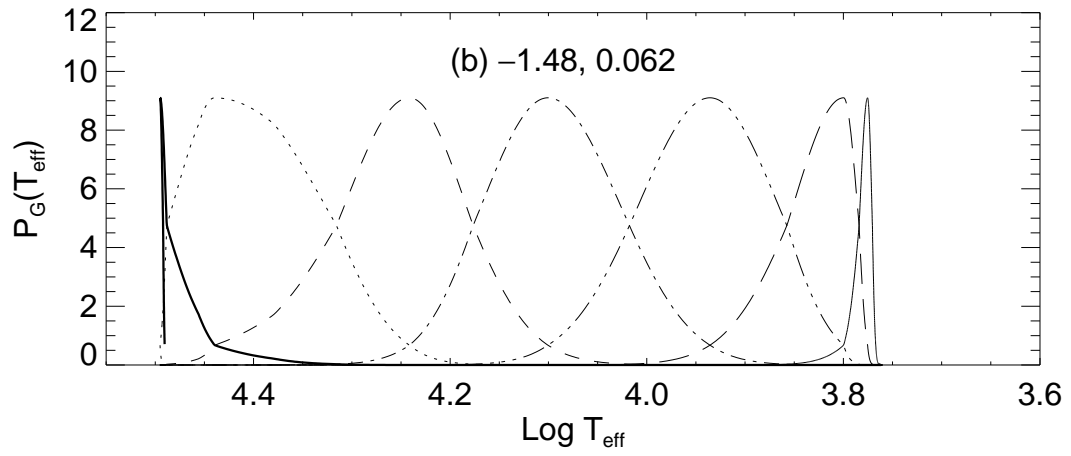
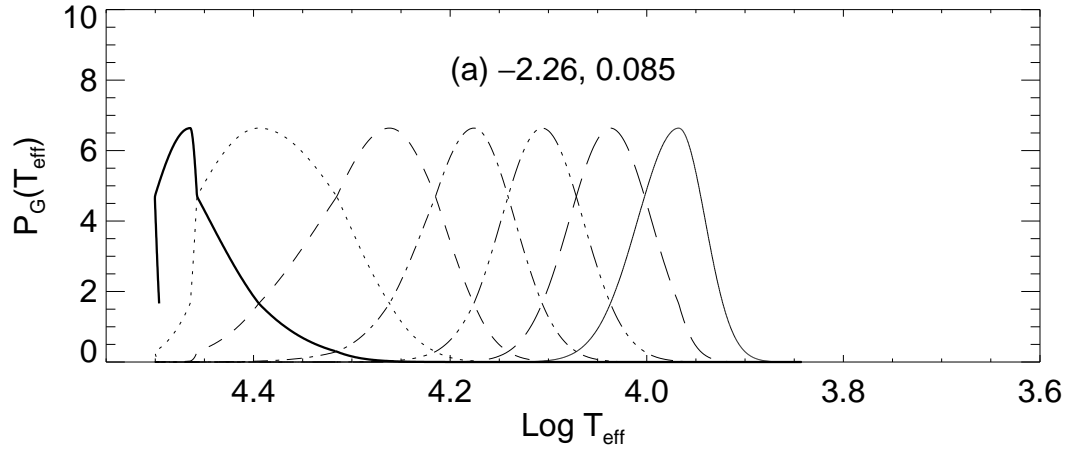
These flat distributions are instructive because they give a measure of the “underlying” effect of mass loss on the stellar mass distribution as the rate is varied. More realistic distributions as found in some clusters resemble gaussians, or at least are unimodal with small dispersion. It is easy to see that such dispersion functions will produce sharply peaked mass distributions if the peak lies at a mass corresponding to either high or low temperature. Figure 8 shows the temperature distributions that result from gaussians of the same width but with different peak locations. The gaussian peaks were chosen relative to η_R (peel – off) and are located at η_R (peel – off) + 0.1, 0.0, –0.1, –0.2, –0.3, –0.4, –0.5. The $\sigma(\eta_R)$ values were chosen such that the width of the corresponding gaussian in mass, $\sigma(M)$, is $0.03M_\odot$ when the gaussian peak is located at η_R (peel – off) – 0.3,. We choose a fiducial width of $0.03M_\odot$ in mass because that is the typical gaussian width of easily modeled globular cluster HBs. For the three lower metallicities the distributions change smoothly as the peak η_R decreases. One can possibly expect to have both RHB and EHB stars using a single Gaussian at these metallicities.

At high Z , the ZAHB distribution is very dependent on the location of the Gaussian peak especially if the peak is located within or near the range of η_R corresponding to the mid-HB region. This is again a consequence of the small range of η_R that corresponds to mid-HB stars in metal rich populations. The ZAHB distribution is insensitive to the Gaussian peak position if the peak is located anywhere within the region corresponding to RHB stars for the high metallicities. Hence at high metallicities one cannot tell the true distribution of the ZAHB if only RHB stars are present. Also, for both RHB and EHB stars to exist in metal rich populations, one has to use a single gaussian which is very broad (much larger than estimated for globular clusters) or use some kind of bimodal distribution.

4. SUMMARY

We have made an extensive study of hot-He-flash stars. These are stars with such high mass loss rates that they peel-off the RGB before He ignition, but rather than quietly becoming He white dwarfs, ignite He while at high T_{eff} . After He ignition the hot-flashers settle on a blue-hook at the hot end of the HB and evolve as EHB stars (DOR95).

In the absence of an alternative, we used the Reimers mass loss formula to compute red giant mass loss rates. We then consider the distribution of initial HB masses as a probability distribution of the Reimers’ efficiency, η_R , rather than directly as a mass probability distribution. The hot-flash behavior was surprisingly widespread. For globular cluster abundances the range of η_R producing EHB stars was comparable to that producing normal HB stars. As metallicity is increased, the range and magnitude of η_R leading to EHB stars varies only slightly, whereas the range of η_R producing mid-HB stars becomes very small. At solar metallicity and higher, the HB will be composed of a group of very hot and very cool stars with little in between so long as nature provides a broad enough distribution in η_R .



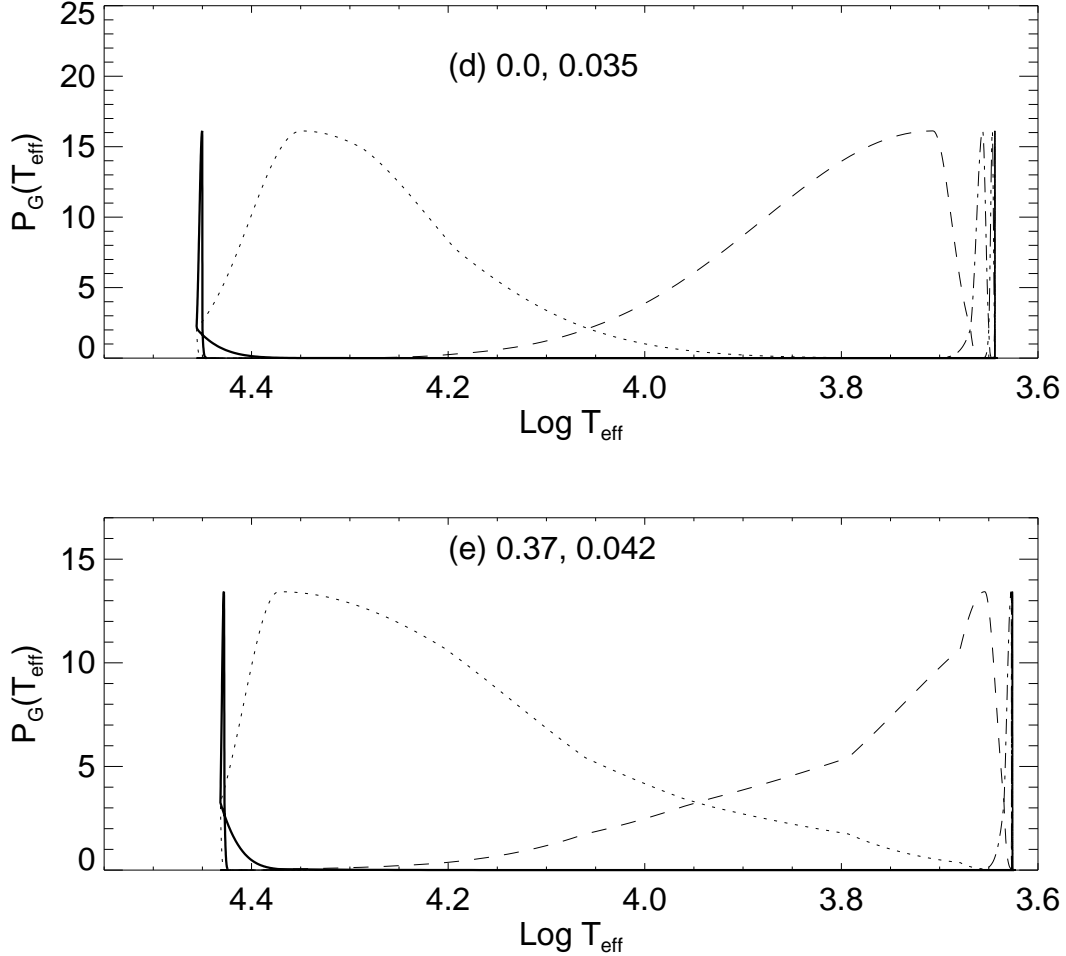


Fig. 8.— The distribution of the gaussian probability density, $P_G(T_{\text{eff}})$, of the effective temperatures for the ZAHB stars. The metallicity and the gaussian width in η_R , $\sigma(\eta_R)$, are listed at the top of each panel. The gaussian peaks are located at $\eta_R(\text{peel} - \text{off}) + 0.1, +0.0, -0.1, -0.2, -0.3, -0.4 - 0.5$, going from left to right. The width $\sigma(\eta_R)$ is set such that it gives a width of $0.03M_{\odot}$ in mass at $\eta_R(\text{peel} - \text{off}) - 0.3$. Note that the gaussian distributions change smoothly at low metallicities for different peak positions. (The vertical lines at the ends of some of the plots are very narrow distributions not fiducial marks.) At high metallicities the distributions change sharply for peaks located in or near the mid-HB region, but the distributions are identical when the peak lies within the RHB.

It has been thought for some time that the upturn in the far-UV spectra of elliptical galaxies and spiral bulges (Burstein et al. 1988) could arise from the UV flux from EHB stars and their progeny (GR90; O’Connell 1993; DRO93; DOR95). The difficulty has been understanding the origin of the EHB stars in metal rich populations. We have shown here that it is just as easy to make EHB stars at high metallicity as at low metallicity. Further, we do not require that the helium abundance continue to grow as steeply with metallicity for $Z > Z_{\odot}$ as is observed at low metallicity ($\Delta Y \sim 3\Delta Z$) (Horch, Demarque, & Pinnsoneault 1992). In claiming that it is just as easy to understand EHB stars in elliptical galaxies as in globular clusters, we have, unfortunately, just passed the buck. We do not really know why some stars in some clusters happen to lose 2–3 times more mass than the typical star. But we do have the comfort of knowing that such stars are observed and the hope that more detailed study of these stars can lead to better understanding of stellar evolution and stellar populations.

NLD thanks Jonathan Whitney for useful discussions. This research was supported by NASA Long Term Astrophysics Grant NAGW-2596, and by NASA RTOP 188-41-51-03.

REFERENCES

- Bailyn, C. D., Sarajedini, A., Cohn, H., Lugger, P., Grindlay, J. E. 1992, *AJ*, 103, 1564
Brocato, E., Matteucci, F., Mazzitelli, I., & Tornambé, A. 1990, *ApJ*, 349, 458
Buonanno, R., Caloi, V., Castellani, V., Corsi, C. E., Fusi Pecci, F., & Gratton, R. 1986, *A&AS*, 66, 79
Burstein, D., Bertola, F. B., Buson, L. M., Faber, S. M., & Lauer, T. R. 1988, *ApJ*, 328, 440
Caputo, F., Chieffi, A., Mazzitelli, I., Tornambé, A., & Castellani, V. 1981, in *IAU Colloq. 68, Astrophysical Parameters for Globular Clusters*, ed. A. G. D. Philip & D. S. Hayes (Dordrecht: Reidel), 313
Castellani, M., & Castellani, V. 1993, *ApJ*, 407, 649 [CC93]
Castellani, V., Degli’Innocenti, S., & Pulone, L. 1995, *ApJ*, 446, 228
Castellani, V., Luridiana, V., Romaniello, M. 1994, *ApJ*, 428, 633
Chiosi, C., & Maeder, A. 1986, *ARAA*, 24, 329
Dorman, B. 1992a, *ApJS*, 81, 221
Dorman, B. 1992b, *ApJS*, 80, 701
Dorman, B., Lee, Y.-W., & Vandenberg, D. A. 1991, *ApJ*, 366, 115
Dorman, B., O’Connell, R. W., & Rood, R. T. 1995, *ApJ*, 442, 105 [DOR95]
Dorman, B., Rood, R. T., & O’Connell, R. W. 1993, *ApJ*, 419, 596 [DRO93]
Dupree, A. K. 1986, *ARAA*, 24, 377
Eggleton, P. P. 1971, *MNRAS*, 151, 351
Ferguson, H. C., & Davidsen, A. F. 1993, *ApJ*, 408, 92
Fusi Pecci, F., & Renzini, A. 1978, *IAU Symposium No. 80, The HR Diagram*, ed. A. G. D. Philip & D. S. Hayes (Dordrecht: Reidel), 225
Green, R. F., Schmidt, M., & Liebert, J. 1986, *ApJS*, 61, 305
Greggio, L., & Renzini, A. 1990, *ApJ*, 364, 35 [GR90]
Han, Z., Podsiadlowski, P., & Eggleton, P. P. 1994, *MNRAS*, 270, 121
Heber, U. 1986, *A&A*, 155, 33
Holzer, T. E., & MacGregor, K. B. 1985, *Mass Loss in Red Giants*, ed. M. Morris & B. Zuckerman (Dordrecht: Reidel), 229
Horch, E., Demarque, P., & Pinnsoneault, M. 1992, *ApJ*, 388, L53
Iben, I., & Rood, R. T. 1970, *ApJ*, 161, 587
Jimenez, R., Jorgensen, U. G., Thejll, P., & MacDonald, J. 1995, *MNRAS*, submitted
Kraft, R. P. 1994, *PASP*, 106, 553
Liebert, J., Saffer, R. A., & Green, E. M. 1994, *AJ*, 107, 1408
Luridiana, V. 1994, *Revista Mexicana de Astronomia y Astrofisica*, 29, 153

- O’Connell, R. W. 1993, in *The Globular Cluster-Galaxy Connection*, ed. G. H. Smith & J. P. Brodie (San Francisco: ASP), 530
- Reimers, D. 1975, *Mém. Soc. Roy. Sci. Liège*, 6^e Ser., 8, 369
- Reimers, D. 1977, *A&A*, 57, 395
- Renzini, A. 1977, in *Advanced Stages of Stellar Evolution Saas-Fee conference*, ed. P. Bouvier & A. Maeder (Geneva: Geneva Obs.), 149
- Renzini, A. 1981, in *Effects of Mass Loss on Stellar Evolution*, ed. C. Chiosi & R. Stalio (Dordrecht: Reidel), 319
- Rood, R. T. 1973, *ApJ*, 184, 815
- Rood, R. T., Crocker, D. A., Fusi Pecci, F., Ferraro, F. R., Clementini, G., & Buonanno, R. 1993, in *The Globular Cluster-Galaxy Connection*, ed. G. H. Smith & J. P. Brodie (San Francisco: ASP), 218
- Saffer, R. A., & Liebert, J. W. 1995, in *Proceedings of the 9th European Workshop on White Dwarfs*, ed. D. Koester & K. Werner (Berlin: Springer), 221
- Schönberner, D. 1979, *A&A*, 79, 108
- Schönberner, D. 1983, *ApJ*, 272, 708
- Spruit, H. C., Nordlund, Å., & Title, A. M. 1990, *ARAA*, 28, 263
- Sweigart, A. V., Mengel, J. G., & Demarque, P. 1974, *A&A*, 30, 13
- Sweigart, A. V., & Gross, P. G. 1978, *ApJS*, 36, 405
- VandenBerg, D. 1983, *ApJS*, 51, 29
- VandenBerg, D. 1992, *ApJ*, 391, 685
- VandenBerg, D., & Bell, R. A. 1985, *ApJS*, 58, 561
- Wheeler, J. C., Sneden, C., & Truran, J. W. 1989, *ARAA*, 27, 279
- Whitney, J. H., et al. 1994, *AJ*, 108, 1350
- Yi, S., Ashfari, E., Demarque, P., & Oemler, A. 1995, *ApJ*, submitted